Simulation Modelling Practice and Theory 111 (2021) 102340

Contents lists available at ScienceDirect

Simulation Modelling Practice and Theory

journal homepage: www.elsevier.com/locate/simpat

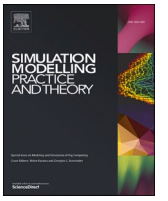

Modified first harmonic approximation-based modeling of SN-compensated inductive power transfer links operating at load-independent-voltage-output frequency

Andrey Vulfovich [a], Dmitry Baimel [b], Alon Kuperman [a,*]

[a] Applied Energy Laboratory, School of Electrical and Computer Engineering, Ben-Gurion University of the Negev, Beer-Sheva, 8410501, Israel.
[b] Department of Electrical and Electronics Engineering, Shamoon College of Engineering, Beer-Sheva, 8410802, Israel.

ARTICLE INFO

Keywords:
Inductive power transfer
series-none compensation
load-independent frequency
first harmonic approximation

ABSTRACT

Some popular applications of wireless power transfer (such as electric vehicle charging) include a transmitter residing on a static platform (charging station) and a dynamic receiver (vehicle). In such applications, compensation may be excluded from the receiver in order to minimize, simplify and lower the cost. If transmitter compensation is also maximally simplified series to none (SN) compensation topology is created. It was recently shown that classical first harmonic approximation (FHA) based analysis fails to accurately predict RMS values of system currents, thus overestimating the achievable coil-to-coil efficiency. Consequently, this paper establishes modified FHA (MFHA) equivalent circuit of SN-compensated inductive power transfer link (IPTL), utilizing analytical expressions of primary and secondary currents based on time-domain differential equations (DE) based solution. It is shown that the outcomes of proposed MFHA and DE methods are very close, justifying the proposed methodology. Simulations and experiments demonstrate excellent matching, validating the presented analysis.

Introduction

Latest progress on the subject of wireless power transfer has shown its appropriateness in applications where traditional wired power transfer is pricey, dangerous or intolerable, owing to flexibility, portability and cord-free operation of the technology [1, 2]. As for today, inductive wireless power transfer, utilizing magnetic field for energy transfer seems to be the most extensively utilized method [3, 4].

A typical IPTL is based on a loosely-coupled transformer (LCT), combined with compensation network/s in order to both increase the efficiency and decrease components' volt-ampere rating. Symmetrical compensation networks on both sides of the LCT are common [5, 6]. Nevertheless, single-static-transmitter multiple-dynamic-receivers applications naturally call for compact, low-cost and lightweight receivers [7, 8]. Series-to-none (SN) and LCL-to-none (LCL-N) [9, 10] compensations were recently proposed to address the need, possessing voltage-source and current-source characteristics, respectively. It was shown that in case of strong coupling, efficiency remains nearly unaffected upon elimination of receiver-side compensation network. This work focuses on SN-compensated ITPL. It was shown in [9] that classical first harmonic approximation (FHA) based analysis [11] fails to accurately predict RMS values of system currents, thus overestimating the achievable coil-to-coil efficiency. As a result, time domain DE-based

* Corresponding author.
E-mail address: alonk@bgu.ac.il (A. Kuperman).

https://doi.org/10.1016/j.simpat.2021.102340
Received 6 January 2021; Received in revised form 6 April 2021; Accepted 28 April 2021
Available online 4 May 2021

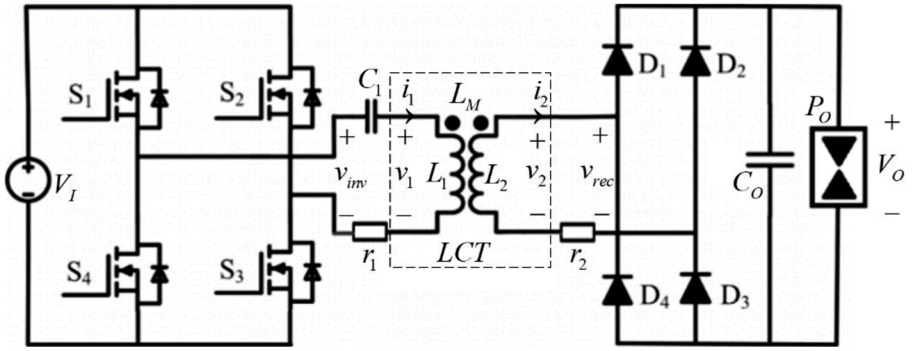

Fig. 1. SN-compensated IPTL

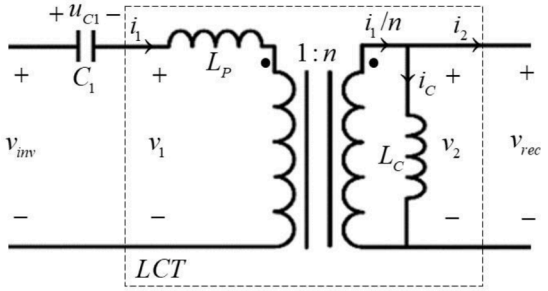

Fig. 2. Equivalent circuit based on alternative ideal-transformer-based LCT representation with SN compensation (r_1 and r_2 are omitted for brevity

solution was used by the authors to obtain performance merits of the compensation topology.

In this paper, analysis of DE-derived expression of the secondary current is shown to contain a significant reactive component in addition to the active one, thus calling for a modified FHA representation of the diode rectifier, which includes a reactive component (namely, an inductor) connected in parallel with the commonly used resistor. In such a representation, the value of equivalent load inductance is proportional to the secondary LCT coil value while independent of other circuit parameters. It is shown that both RMS currents and hence coil-to-coil efficiency obtained using DE and the proposed MFHA methods are very close, justifying the use of the proposed methodology. The findings are verified by simulations and experiments, demonstrating the feasibility of proposed modeling approach.

SN-Compenstaed IPTL operating in load independent voltage output regime

Power loaded SN-compensated IPTL is depicted in Fig. 1, where V_I and V_O denote input and output DC voltages, L_1 and L_2 symbolize primary and secondary inductances, C_1 represents primary compensating capacitance, r_1 and r_2 signify equivalent primary and secondary resistances, $0 \leq k = L_M/\sqrt{L_1 L_2} \leq 1$ denotes coupling coefficient with L_M indicating mutual inductance of loosely-coupled transformer (LCT) coils and C_O and P_O stand for load filter capacitance and power, respectively. Inverter output voltage is given by

$$v_{inv}(t) = \begin{cases} V_I, & 0 < \omega t \leq \pi \\ -V_I & \pi < \omega t \leq 2\pi \end{cases} \tag{1}$$

with $\omega = 2\pi f = 2\pi/T$ denoting constant operational frequency. Assuming the diode rectifier operates in continuous conduction mode (CCM), its input voltage is expressed by

$$v_{rec}(t) = \begin{cases} V_O, & \theta < \omega t \leq \pi + \theta \\ -V_O & \pi + \theta < \omega t \leq 2\pi + \theta \end{cases}. \tag{2}$$

Input-output relations of the LCT in Fig. 2 are given by [12]

$$\begin{aligned} v_1(t) &= L_1 \frac{di_1(t)}{dt} - L_M \frac{di_2(t)}{dt} \\ v_2(t) &= -L_2 \frac{di_2(t)}{dt} + L_M \frac{di_1(t)}{dt}. \end{aligned} \tag{3}$$

It was recently shown in [13] that infinite amount of possible ideal-transformer-based LCT representations exist in general. In this

paper, phasor-domain equivalent circuit shown within dashed box in Fig. 2 (i.e. all the variables are FHA representations of corresponding signals) is considered with [14]

$$L_P = L_1\left(1-k^2\right), \quad L_C = L_2, \quad n = \frac{1}{k}\sqrt{L_2 L_1^{-1}} = \frac{L_2}{L_M}. \tag{4}$$

Consequently, selecting the value of compensating capacitor C_1 as

$$C_1 = \frac{1}{\omega^2 L_P} = \frac{1}{\omega^2 L_1\left(1-k^2\right)} \tag{5}$$

to resonate with L_P yields (neglecting r_1 and r_2) $\theta = 0$ in (2). In addition, the voltage gain becomes load-independent [15, 16], given by

$$\frac{\left|\overrightarrow{v}_{rec}\right|}{\left|\overrightarrow{v}_{inv}\right|} = n = \frac{1}{k}\sqrt{L_2 L_1^{-1}} = \frac{L_2}{L_M} \tag{6}$$

with $\overrightarrow{x}$ indicating that x is a phasor. Note that peak values are used for phasor notations in the paper

A. Classical FHA-based analysis

According to the classical FHA-based analysis [11], DC-side quantities are related to corresponding FHA AC-side counterparts as

$$\left|\overrightarrow{v}_{inv}\right| = \frac{4}{\pi}V_I, \quad \left|\overrightarrow{v}_{rec}\right| = \frac{4}{\pi}V_O, \quad \frac{\overrightarrow{v}_{rec}}{\overrightarrow{i}_2} = R_L = \frac{8}{\pi^2}R_O = \frac{8}{\pi^2}\frac{V_O^2}{P_O}, \tag{7}$$

i.e. the diode rectifier is represented by pure resistance. Hence, secondary current is given by

$$\overrightarrow{i_2} = \frac{\pi I_O}{2} + j0 = \frac{\pi V_O}{2\omega L_2}\frac{\omega L_2}{R_O} + j0 = \frac{\pi V_O}{2\omega L_2} ctg\beta \measuredangle 0 \tag{8}$$

with

$$tg\beta = \frac{R_O}{\omega L_2} \tag{9}$$

denoting the load matching factor. Referring to Fig. 2 and (7), the current flowing through L_C is given by

$$\overrightarrow{i_C} = \frac{\frac{4}{\pi}V_O}{j\omega L_2} = \frac{\frac{4}{\pi}V_O}{\omega L_2}\measuredangle(-0.5\pi) \tag{10}$$

and hence (cf. 6)

$$\frac{\overrightarrow{i_1}}{n} = \overrightarrow{i_2} + \overrightarrow{i_C} \Rightarrow \overrightarrow{i}_1 = \frac{\pi V_O}{2\omega L_M}\sqrt{\left(\frac{8}{\pi^2}\right)^2 + ctg^2\beta}\measuredangle(-\delta) \tag{11}$$

with

$$\delta = tg^{-1}\left(\frac{8}{\pi^2}tg\beta\right). \tag{12}$$

Consequently, RMS values of primary and secondary currents are obtained as

$$I_{1,RMS} = \frac{\pi V_O}{2\sqrt{2}\omega L_M}\sqrt{ctg^2\beta + \left(\frac{8}{\pi^2}\right)^2}, \quad I_{2,RMS} = \frac{\pi V_O}{2\sqrt{2}\omega L_2} ctg\beta, \tag{13}$$

respectively. Coil-to-coil efficiency is given by

$$\eta = \frac{P_O}{P_O + I_{1,RMS}^2 r_1 + I_{2,RMS}^2 r_2} = \frac{1}{1 + \frac{I_{1,RMS}^2 r_1 + I_{2,RMS}^2 r_2}{P_O}} \tag{14}$$

with

$$P_O = I_O^2 R_O = \frac{V_O^2}{R_O}. \tag{15}$$

Defining quality factors of the primary and secondary LCT coils as

$$Q_1 = \frac{\omega L_1}{r_1}, \quad Q_2 = \frac{\omega L_2}{r_2}, \tag{16}$$

respectively, and combining (13) – (16) yields

$$\eta_{SN,1} \cong \frac{1}{1 + \frac{\pi^2}{8}\frac{1}{tg\beta}\left(\frac{1}{k^2}\left(1 + \left(\frac{8}{\pi^2}\right)^2 tg^2\beta\right)Q_1^{-1} + Q_2^{-1}\right)}. \tag{17}$$

Further assuming that $Q_1 = Q_2 = Q$ reduces (17) to

$$\eta_{SN,1} \cong \frac{1}{1 + \frac{\pi^2}{8}\frac{1}{k^2 Q tg\beta}\left(1 + \left(\frac{8}{\pi^2}\right)^2 tg^2\beta + k^2\right)}, \tag{18}$$

maximized at

$$(tg\beta)^* = \frac{\pi^2}{8}\sqrt{1 + k^2} \tag{19}$$

as

$$\eta^*_{SN,1} \cong \frac{1}{1 + \sqrt{1 + \frac{1}{k^2}}\frac{2}{kQ}}. \tag{20}$$

B. *Differential equations based analysis*

Time domain behavior the system is described by

$$\begin{cases} L_C \dfrac{d\left(\dfrac{i_1(t)}{n} - i_2(t)\right)}{dt} = \begin{cases} V_O, & 0 < \omega t \le \pi \\ -V_O, & \pi < \omega t \le 2\pi \end{cases} \\ L_P \dfrac{di_1(t)}{dt} + u_{C1}(t) = \begin{cases} V_I - \dfrac{V_O}{n}, & 0 < \omega t \le \pi \\ \dfrac{V_O}{n} - V_I, & \pi < \omega t \le 2\pi \end{cases} \\ i_1(t) = C_1 \dfrac{du_{C1}(t)}{dt} \end{cases} \tag{21}$$

with following initial conditions,

$$\begin{aligned} &i_1(0) = -i_1(\pi) = i_1(2\pi) \\ &i_2(0) = i_2(\pi) = i_2(2\pi) = 0 \\ &u_{C1}(0) = -u_{C1}(\pi) = u_{C1}(2\pi). \end{aligned} \tag{22}$$

Solving (21) with (22) and (5) yields, after substituting the parameters in (4), primary and secondary side currents [9]

$$\begin{aligned} i_1(t) &= \frac{\pi V_O}{2\omega L_M}\sqrt{1 + ctg^2\beta}\sin(\omega t - \beta), \\ i_2(t) &= \frac{\pi V_O}{2\omega L_2}\sqrt{1 + ctg^2\beta}\sin(\omega t - \beta) - \frac{V_O}{\omega L_2}\cdot \begin{cases} \left(\omega t - \dfrac{\pi}{2}\right), & 0 < \omega t \le \pi \\ -\left(\omega t + \dfrac{\pi}{2}\right), & \pi < \omega t \le 2\pi \end{cases}, \end{aligned} \tag{23}$$

respectively. The last term of $i_2(t)$ is actually a triangular wave, hence it may be replaced by corresponding Fourier series as

$$i_2(t) = \frac{\pi V_O}{2\omega L_2}\sqrt{1 + ctg^2\beta}\sin(\omega t - \beta) \quad + \frac{\pi V_O}{2\omega L_2}\frac{8}{\pi^2}\sum_{n=1,odd}^{\infty}\frac{1}{n^2}\sin\left(\frac{\pi n}{2}\right)^2\cos(n\omega t). \tag{24}$$

Hence, the first harmonic of secondary current is given by

$$i_{21}(t) = \frac{\pi V_O}{2\omega L_2}\sqrt{1+ctg^2\beta}\sin(\omega t-\beta) + \frac{\pi V_O}{2\omega L_2}\frac{8}{\pi^2}\cos(\omega t) = \frac{\pi V_O}{2\omega L_2}\sqrt{ctg^2\beta+\left(1-\frac{8}{\pi^2}\right)^2}\sin(\omega t-\lambda) \tag{25}$$

with

$$\lambda = tg^{-1}\left(\left(1-\frac{8}{\pi^2}\right)tg\beta\right), \tag{26}$$

i.e. (24) may be rewritten as

$$i_2(t) = \frac{V_O\pi}{2\omega L_2}\sqrt{ctg^2\beta+\left(1-\frac{8}{\pi^2}\right)^2}\sin(\omega t-\lambda) + \frac{V_O\pi}{2\omega L_2}\frac{8}{\pi^2}\sum_{n=3,odd}^{\infty}\frac{1}{n^2}\sin\left(\frac{\pi n}{2}\right)^2\cos(n\omega t). \tag{27}$$

RMS values of primary and secondary currents are obtained as

$$I_{1,RMS} = \frac{V_O\pi}{2\sqrt{2}\omega L_M}\sqrt{1+ctg^2\beta}, I_{2,RMS} = \frac{V_O\pi}{2\sqrt{2}\omega L_2}\sqrt{\left(1\frac{2}{3}-2\frac{8}{\pi^2}\right)+ctg^2\beta}, \tag{28}$$

respectively. Obviously, both RMS values in (28) are underestimated by (13). Combining (28) with (14) – (16) yields coil–to-coil efficiency given by

$$\eta_{SN} \cong \frac{1}{1+\frac{\pi^2}{8}\frac{1}{tg\beta}\left(\frac{1+tg^2\beta}{k^2}Q_1^{-1}+\left(1+\left(1\frac{2}{3}-2\frac{8}{\pi^2}\right)tg^2\beta\right)Q_2^{-1}\right)}. \tag{29}$$

In case $Q_1 = Q_2 = Q$, (29) reduces to

$$\eta_{SN} \cong \frac{1}{1+\frac{\pi^2}{8}\frac{1}{Qtg\beta}\left(\frac{1+tg^2\beta}{k^2}+\left(1+\left(1\frac{2}{3}-2\frac{8}{\pi^2}\right)tg^2\beta\right)\right)}, \tag{30}$$

maximized at

$$(tg\beta)^* = \sqrt{\frac{1+k^2}{1+k^2\left(1\frac{2}{3}-2\frac{8}{\pi^2}\right)}} \tag{31}$$

as

$$\eta_{SN}^* \cong \frac{1}{1+\frac{\pi^2}{8}\sqrt{1+k^2\left(1\frac{2}{3}-2\frac{8}{\pi^2}\right)}\sqrt{1+\frac{1}{k^2}}\frac{2}{kQ}}. \tag{32}$$

Note that since

$$1\frac{2}{3}-2\frac{8}{\pi^2} = 0.0455, \tag{33}$$

then

$$\eta_{SN}^* \approx \frac{1}{1+\frac{\pi^2}{8}\sqrt{1+\frac{1}{k^2}}\frac{2}{kQ}} \approx 1-\frac{\pi^2}{8}\left(1-\eta_{SN,1}^*\right)\left\langle\eta_{SN,1}^*, \right. \tag{34}$$

i.e. the efficiency is overestimated by FHA-based analysis.

C. Modified FHA-based analysis

The above analysis indicates that classical FHA-based analysis fails to accurately predict the coil-to-coil efficiency of SN-compensated IPTL. Time-domain analysis discloses that secondary current contains reactive component as well as triangular wave-related high-order harmonics. While the latter may be ignored due to negligible contribution to RMS value of the secondary current, reactive component impact is significant. Since classical FHA-based analysis represents the diode rectifier by a pure resistor, reactive component of secondary current is automatically neglected, underestimating the losses caused by the increase in RMS value of current due to additional reactive component presence. Rewriting (25) as

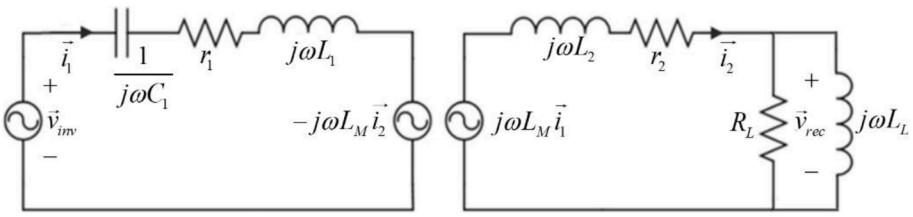

Fig. 3. Modified FHA-based representation of SN-compensated IPTL

$$i_{21}(t) = \frac{\pi V_O}{2\omega L_2} ctg\beta \sin(\omega t) + \frac{\pi V_O}{2\omega L_2}\left(1 - \frac{8}{\pi^2}\right)\cos(\omega t) \quad = \frac{\frac{4}{\pi}V_O}{\frac{8}{\pi^2}R_O}\sin(\omega t) + \frac{\frac{4}{\pi}V_O}{\frac{8}{\pi^2-8}\omega L_2}\cos(\omega t) \tag{35}$$

indicates, that the diode rectifier representation should be modified so that it is replaced by the resistor R_L in (7), connected in parallel with an inductance $L_L = 8L_2/(\pi^2\text{-}8)$, as shown in Fig. 3 in order to take into account the reactive component present and provide a more accurate estimate of the secondary current when compared to (8). Note that while the resistor is load-dependent, the inductance depends solely on the value of L_2. Taking this finding into account, the secondary current expression in (8) should be modified as

$$\overrightarrow{i_2} = \frac{\pi I_O}{2} + \frac{\frac{4}{\pi}V_O}{j\omega L_L} = \frac{\pi V_O}{2\omega L_2} ctg\beta - \frac{\frac{4}{\pi}V_O}{j\omega\frac{8}{\pi^2-8}L_2} = \frac{\pi V_O}{2\omega L_2}\sqrt{ctg^2\beta + \left(1 - \frac{8}{\pi^2}\right)^2}\measuredangle\lambda \tag{36}$$

and (11) becomes

$$\frac{\overrightarrow{i_1}}{n} = \overrightarrow{i_2} + \overrightarrow{i_C} \Rightarrow \overrightarrow{i}_1 = \frac{L_2}{L_M}\left(\frac{\pi V_O}{2\omega L_2} ctg\beta - j\frac{\pi V_O}{2\omega L_2}\right) = \frac{\pi V_O}{2\omega L_M}\sqrt{1 + ctg^2\beta}\measuredangle(-\beta). \tag{37}$$

Modified RMS values of primary and secondary currents are obtained as

$$I_{1,RMS} = \frac{\pi V_O}{2\sqrt{2}\omega L_M}\sqrt{1 + ctg^2\beta}, I_{2,RMS} = \frac{\pi V_O}{2\sqrt{2}\omega L_2}\sqrt{ctg^2\beta + \left(1 - \frac{8}{\pi^2}\right)^2}, \tag{38}$$

respectively. The coil–to-coil efficiency is then given by (cf. (12) – (14))

$$\eta_{SN,1} \cong \frac{1}{1 + \frac{\pi^2}{8}\frac{1}{ctg\beta}\left(\frac{1+ctg^2\beta}{k^2}Q_1^{-1} + \left(ctg^2\beta + \left(1 - \frac{8}{\pi^2}\right)^2\right)Q_2^{-1}\right)}. \tag{39}$$

Assuming that $Q_1 = Q_2 = Q$ (39) reduces to

$$\eta_{SN,1} \cong \frac{1}{1 + \frac{\pi^2}{8}\frac{1}{Qtg\beta}\left(\frac{1}{k^2}(1 + tg^2\beta) + \left(1 + \left(1 - \frac{8}{\pi^2}\right)^2 tg^2\beta\right)\right)}, \tag{40}$$

maximized at

$$(tg\beta)^* = \sqrt{\frac{1 + \frac{1}{k^2}}{\left(1 - \frac{8}{\pi^2}\right)^2 + \frac{1}{k^2}}} \tag{41}$$

as

$$\eta^*_{SN,1} \cong \frac{1}{1 + \frac{\pi^2}{8}\frac{2}{Q}\sqrt{\left(1 + \frac{1}{k^2}\right)\left(\frac{1}{k^2} + \left(1 - \frac{8}{\pi^2}\right)^2\right)}}. \tag{42}$$

Since

$$\left(1 - \frac{8}{\pi^2}\right)^2 = 0.0359 << \frac{1}{k^2} \tag{43}$$

for practical values of k, then

Table I
System parameter values

Parameter	Value	Units
V_I	270	V
L_1	180	μH
L_2	180	μH
k	0.71	–
r_1	2	Ω
r_2	2	Ω
Q_1	70	–
Q_2	70	–
C_O	660	μF

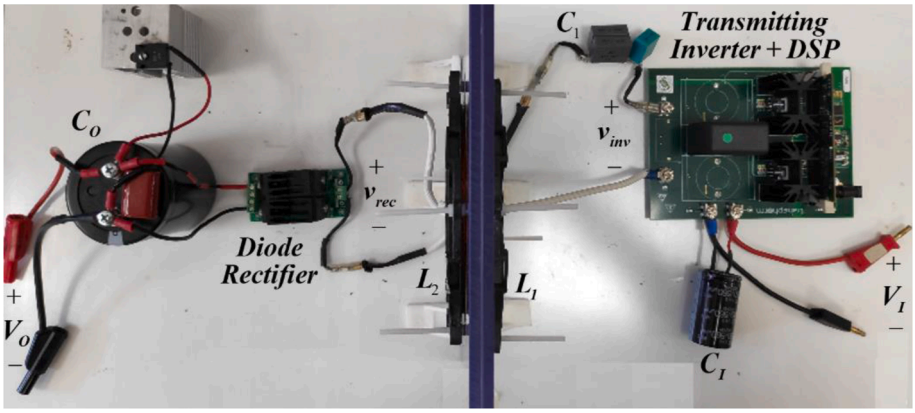

Fig. 4. Experimental setup.

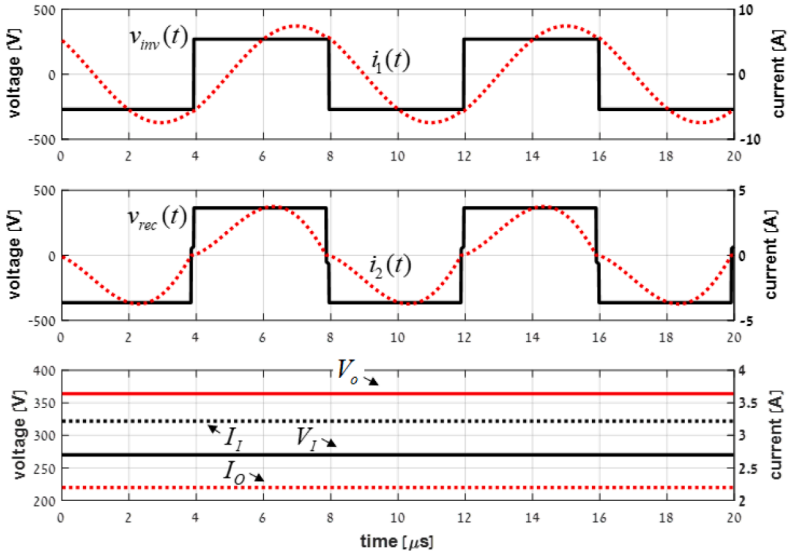

Fig. 5. Time-domain simulation results, $P_O = 800$W.

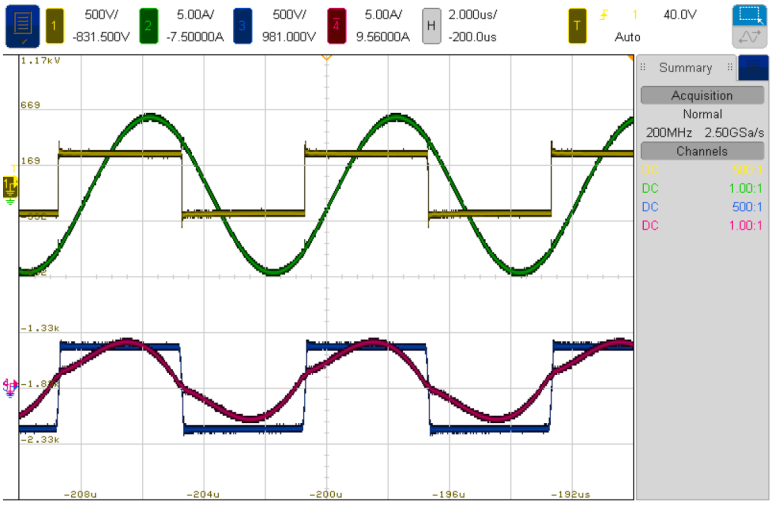

(a) AC-side signals

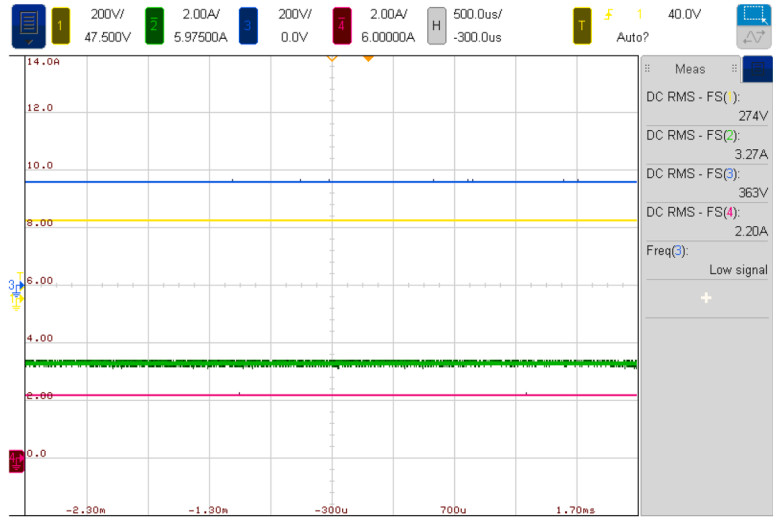

(b) DC-side signals

Fig. 6. Time-domain experimental results, $P_O = 800$W.

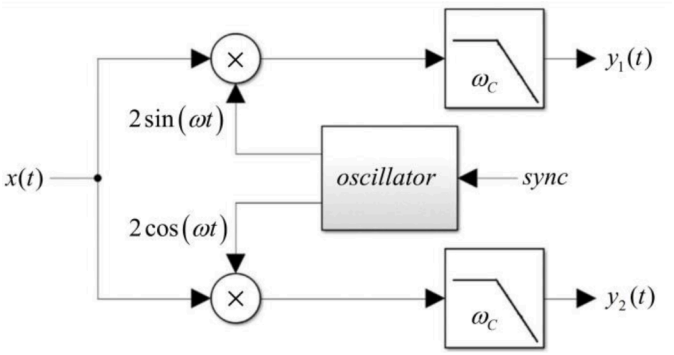

Fig. 7. Quadrature Demodulator

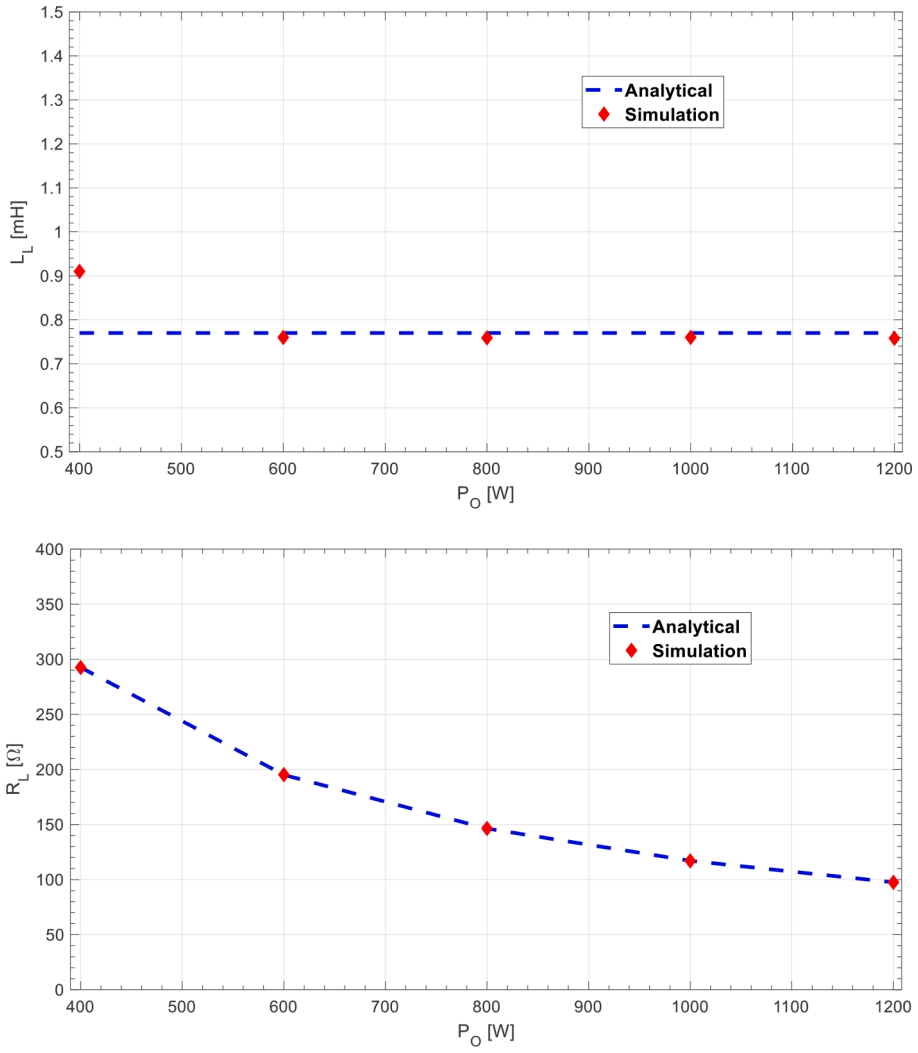

Fig. 8. Components of rectifier modified FHA equivalent circuit versus load power

$$\eta^*_{SN,1} \approx \frac{1}{1+\frac{\pi^2}{8}\sqrt{1+\frac{1}{k^2}}\,\frac{2}{kQ}} = \eta^*_{SN}, \tag{44}$$

i.e. coil-to-coil efficiency is accurately estimated by the proposed modified FHA-based analysis.

Validation

Consider a SN-compensated inductive IPTL with parameter values summarized in Table I, feeding loads in range of 400W $< P_O <$ 1200W with the maximum efficiency desired at output power level of 800W. According to (6), expected idealized DC-side output WPTL voltage is $V_O = 380$V. Optimal load matching factor is obtained from (29) as $(tg\beta)^* = 1.21$, while equivalent DC-side resistance at 800W is $R_O = (V_O)^2/P_O \approx 144\Omega$. Consequently, operating frequency is selected according to (9) as $\omega = 2\pi \cdot 124{,}500$rad/s and the value of compensation capacitor is set to (cf. (5)) $C_1 = 17.8$nF. According to (42) and Table I, expected maximized coil-to-coil efficiency at 800W loading is 92.1%.

The WPTL was simulated using PSIM software. The LCT was modelled by equivalent circuit shown in Fig. 2 in order to verify the derived analytical expressions of system currents. In order to experimentally validate the presented analysis, SN-compensated WPTL with parameters matching Table I was built and tested. Transmitting-side inverter was realized using 650V, 150mΩ TPH3206PSB transistors driven by SI8273AB1 drivers. Switching signals were supplied by Texas Instruments F28335 digital signal processor-based control card. Receiving-side rectifier was built utilizing APT40DQ60BG diodes. The WPTL was powered from IT61517D ITECH power supply and terminated by Maynuo M9715B electronic load, operated in constant power mode.

Experimental setup is depicted in Fig. 4. Typical simulation and experimental time-domain waveforms (under optimal 800W

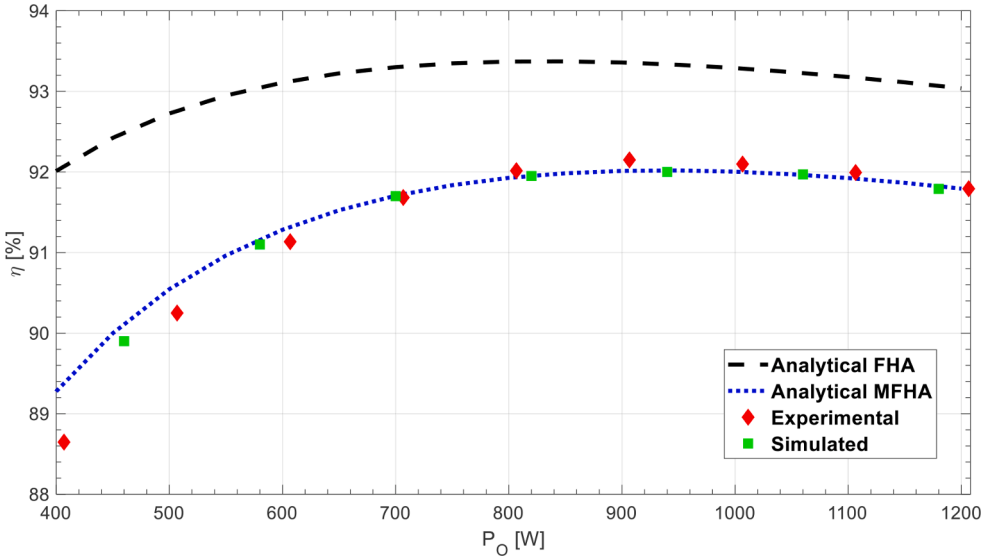

Fig. 9. Efficiency versus load power

loading) are shown in Figs. 5 and 6, respectively, demonstrating close match.

In order to verify that the value of equivalent resistance R_L is output power dependent while the value of equivalent inductance L_L is load independent, rectifier input current and voltage were fed into a quadrature demodulator [17], shown in Fig. 7. For the input given by

$$x_1(t) = X_1\cos(\omega t + \psi_1) \Rightarrow \overrightarrow{x}_1 = \underbrace{X_1\cos\psi_1}_{X_{1R}} + j\underbrace{X_1\sin\psi_1}_{X_{1I}} = X_{1R} + jX_{1I}, \tag{45}$$

demodulator output is given by

$$\overrightarrow{y} = \begin{cases} y_1(t) = X_{1R} \\ y_2(t) = X_{1I} \end{cases}, \tag{46}$$

allowing to obtain the in-phase and quadrature components of the secondary current (35).

Calculated equivalent resistance and inductance are given in Fig. 8. It may be concluded that as long as the rectifier operates in CCM, the proposed analysis outcomes are valid. Under 400W loading, the rectifier operates in DCM and the equivalent inductance slightly increases, as predicted in [17].

Experimental coil-to-coil efficiency versus load power are shown in Fig. 9 along with corresponding classical and modified FHA (MFHA) based analytical predictions obtained using (30) and (40). It is well-evident that while the former overestimates the efficiency, the latter yields and accurate prediction. Optimal values of load matching factor and efficiency are also validated.

Conclusion

In this work, SN-compensated IPTL featuring a compact structure of a non-compensated transmitter, was studied. It was shown that classical FHA-based analysis fails to accurately predict RMS values of system currents, leading to coil-to-coil efficiency overestimation. Consequently, modified FHA-based circuit was derived, based on DE-based approach outcomes. It was shown that load-independent-valued inductance should be added in parallel to the commonly used resistance to significantly increase the accuracy of rectifier FHA model. Simulation and experimental results demonstrated good matching, supporting the proposed modified FHA representation of SN compensation topology.

References

[1] C.C. Mi, G. Buja, S.Y. Choi, C.T. Rim, Modern advances in wireless power transfer systems for roadway powered electric vehicles, IEEE Trans. Ind. Electron. 63 (10) (Oct. 2016) 6533–6545.
[2] Z. Zhang, H. Pang, A. Georgiadis, C. Cecati, Wireless power transfer – An overview, IEEE Trans. Ind. Electron. 66 (2) (Feb. 2019) 1044–1058.
[3] A. Seitaridis, E.S. Rigas, N. Bassiliades, S.D. Ramchurn, An agent-based negotiation scheme for the distribution of electric vehicles across a set of charging stations, Simul. Modell. Pract. Theory 100 (2020). Article 102040.
[4] S. Lhazmir, O.A. Oualhaj, A. Kobbane, L. Mokdad, A decision-making analysis in UAV-enabled wireless power transfer for IoT networks, Simul. Modell. Pract. Theory 103 (Sep. 2020), 102102.
[5] W. Zhang, C.C. Mi, Compensation topologies of high-power wireless power transfer systems, IEEE Trans. Veh. Technol. 65 (6) (Jun. 2016) 4768–4778.

[6] E.S. Rigas, S. Karapostolakis, N. Bassiliades, S.D. Ramchurn, EVLibSim: A tool for the simulation of electric vehicles' charging stations using the EVlib library, Simul. Modell. Pract. Theory 87 (2018) 99–119.
[7] B. Esteban, N. Sid-Ahmed, N.C. Kar, A comparative study of power supply architectures in wireless EV charging systems, IEEE Trans. Power Electron. 30 (22) (Nov. 2015) 6408–6422.
[8] I.I. Nam, R.A. Dougal, E. Santi, Novel unity-gain frequency control of series-series resonant converter to improve efficiency and receiver positioning flexibility in wireless charging of portable electronics, IEEE Trans. Ind. Appl. 51 (1) (2015) 385–397. Jan./Feb.
[9] Y. Zhang, et al., Modeling and analysis of series-none compensation for wireless power transfer systems with a strong coupling, IEEE Trans. Power Electron. 34 (2) (Feb. 2019) 1209–1215.
[10] Y. Zhang, et al., A high-power wireless charging system using LCL-N topology to achieve a compact and low-cost receiver, IEEE Trans. Power Electron. 35 (1) (Jan. 2020) 131–137.
[11] R.L. Steigerwald, A comparison of half-bridge resonant converter topologies, IEEE Trans. Power Electron. 3 (2) (Feb. 1988) 174–182.
[12] D. Baimel, A. Kuperman, Multi-regional modeling and operational analysis of LC/S-compensated inductive wireless power transfer link with load-independent current output, Simul. Modell. Pract. Theory 105 (Jul. 2020), 102154.
[13] A. Kuperman, Compensation capacitors sizing for achieving arbitrary load-independent voltage gain in series-series inductive WPT link operating at fixed frequency, IEEE Trans. Power Delivery 35 (6) (Dec. 2020) 2737–2739.
[14] A. Kuperman, Comment on 'Analysis, design, and optimization of LC/S compensation topology with excellent load-independent voltage output for inductive power transfer, IEEE Trans. Transp. Electrificat. 5 (4) (Dec. 2019) 1480–1483.
[15] Y. Frechter, A. Kuperman, Output voltage range of power loaded series-series compensated inductive wireless power transfer link operating in load-independent regime, IEEE Trans. Power Electron. 35 (6) (Jun. 2020) 6586–6593.
[16] O. Knecht, R. Bosshard, J.W. Kolar, High-efficiency transcutaneous energy transfer for implantable mechanical heart support systems, IEEE Trans. Power Electron. 30 (11) (Nov. 2015) 6221–6236.
[17] O. Trachtenberg, et al., Quadrature demodulator based output voltage and load estimation of a resonant inductive WPT link, in: Proc. *IEEE PELS Workshop on Emerging Technologies: Wireless Power Transfer (WoW)*, London, UK, 2019. Jun. 17 –21.